AIP | Journal of Applied Physics

Fundamental properties of field emission-driven direct current microdischarges

Paul Rumbach and David B. Go

Citation: J. Appl. Phys. **112**, 103302 (2012); doi: 10.1063/1.4764344
View online: http://dx.doi.org/10.1063/1.4764344
View Table of Contents: http://jap.aip.org/resource/1/JAPIAU/v112/i10
Published by the American Institute of Physics.

Fundamental properties of field emission-driven direct current microdischarges

Paul Rumbach and David B. Go[a)]
Department of Aerospace and Mechanical Engineering, University of Notre Dame, Notre Dame, Indiana 46556, USA

(Received 2 July 2012; accepted 12 October 2012; published online 21 November 2012)

For half a century, it has been known that the onset of field emission in direct current microdischarges with gap sizes less than 10 μm can lead to breakdown at applied voltages far less than predicted by Paschen's law. It is still unclear how field emission affects other fundamental plasma properties at this scale. In this work, a one-dimensional fluid model is used to predict basic scaling laws for fundamental properties including ion density, electric field due to space charge, and current-voltage relations in the pre-breakdown regime. Computational results are compared with approximate analytic solutions. It is shown that field emission provides an abundance of cathode electrons, which in turn create large ion concentrations through ionizing collisions well before Paschen's criterion for breakdown is met. Breakdown due to ion-enhanced field emission occurs when the electric field due to space charge becomes comparable to the applied electric field. Simple scaling analysis of the 1D Poisson equation demonstrates that an ion density of $n_+ \approx 0.1V_A\varepsilon_0/qd^2$ is necessary to significantly distort the electric field. Defining breakdown in terms of this critical ion density leads analytically to a simple, effective secondary emission coefficient γ' of the same mathematical form initially suggested by Boyle and Kisliuk [Phys. Rev. **97**, 255 (1955)]. © *2012 American Institute of Physics*. [http://dx.doi.org/10.1063/1.4764344]

I. INTRODUCTION

Microplasmas and microdischarges—defined as discharges having characteristic lengths less than 1 mm—continue to receive significant attention because of their stability at atmospheric pressures, high electron and ion densities, and non-Maxwellian electron energy distributions that lead to a vast set of applications including lighting, chemical synthesis, environmental sensing, and material processing.[2] There are still many questions that exist about the fundamental nature of these discharges and how they are similar to or different from their macroscale counterparts. One of the key byproducts of scaling discharges down is that the surface-to-volume ratio necessarily increases. This can have multiple effects on the discharge thermodynamics, influencing both the energy balance and the energy distribution in the discharge.[3] It is clear, therefore, that as surfaces play a more prominent role in the operation of discharges at the microscale, it is necessary to more completely understand electrode processes such as electron emission, and, ultimately, how to control these processes.

One area of microdischarges where surface effects have played an important role is microscale breakdown for electrode gaps below ~7 μm. For over half a century, it has been known that Paschen's law fails at the micron-scale due to electron field emission.[1] This phenomenon occurs when electric fields become sufficiently large so that electrons begin to tunnel out of the cathode into the discharge. In 2002, Slade and Taylor stated that the mechanism for breakdown in gaps less than 4 μm is similar to that of vacuum breakdown and is primarily the result of field emission from micro-protrusions on the cathode surface, which enhance the electric field by a factor β.[4] Another model for microscale breakdown, known as *ion-enhanced field emission*, holds that, in addition to geometric enhancement, the electric field at the cathode is also enhanced by the presence of positive, ionic space charge. Field emitted electrons create an abundance of ions through collisional processes. These ions increase the field at the cathode, inducing greater field emission. This feedback mechanism ultimately leads to breakdown at applied voltages lower than those predicted by Paschen's law or vacuum breakdown theory. In 2007, Radmilović and Radjenović used particle-in-cell/Monte Carlo collision (PIC/MCC) simulations to show that field emission in micro-scale gaps leads to these lower breakdown voltages by producing an excess of ionizations.[5] In 2010, Tirumala and Go analytically derived an effective secondary emission coefficient, γ, that takes into account both secondary (Auger) emission, γ_i, and ion-enhanced field emission, γ'. Using this modified secondary emission coefficient, they were able to analytically produce a modified Paschen's curve that predicts the deviations from Paschen's law seen in experiment.[6] It should be noted that there has been some dispute about the role of field emission during breakdown as other mechanisms such as a long path effects can be important.[7] But it is generally accepted that field emission plays an important role in extremely small gap dimensions (<7 μm).

Because of its effect on breakdown, it is reasonable to anticipate that field emission will serve as a significant source of free electrons and will actually alter the way a discharge operates as well as its fundamental properties in regimes other than the breakdown point. For example, Kim

[a)]Author to whom correspondence should be addressed. email: dgo@nd.edu.

et al. used a two-dimensional PIC/MCC simulation to show that carbon nanotube (CNT) field-emitters significantly alter the structure and greatly reduce the cathode sheath potential of a micro-hollow cathode discharge.[8] Similarly, researchers from the University of Illinois, Urbana-Champagne have used doped silicon pn-junctions[9,10] to control the production of field-emitted electrons and quench microplasma on demand. They have also shown experimentally that incorporating CNTs on the cathode of a microhollow cathode device on the scale of 100 μm significantly decreased the ignition voltage and allowed for sustaining voltages as low as 109 V for neon at pressures greater than 300 Torr, attributing this to field emission.[11] A number of studies have also utilized various cathode materials such as CNT films,[12] diamond,[13,14] nickel,[15] gold,[16] and gold nanorods[17] to promote field emission. These devices operate at moderate pressures (atmospheric and near-atmospheric), but *below the breakdown threshold*, and often generate appreciable current ($\sim$nA to μA). This field emission approach has been used to create gas sensors[18,19] and ionization devices for chemical analysis.[20]

What these results suggest is that there is potentially a new discharge regime driven by field emission and enabled by the microscale. Since most of these field emission devices operate below the breakdown threshold, the authors propose the name of "field emission-driven Townsend microdischarges" to describe the regime in which they operate. Yet, besides the work involving breakdown and the modified Paschen's curve, very little effort has been given to determine fundamental properties of field emission-driven Townsend microdischarges. Further, there has been little effort to elucidate the implications of ion-enhanced field emission as an additional, dominant cathode process. In this work, a one-dimensional fluid model is used to explore this interesting regime. Not only does the model highlight the impact of ion-enhanced field emission on discharge properties such as current density, ion density, and electric field, but it also reveals the importance of positive space charge on ion-enhanced field emission and ultimately breakdown. This analysis leads to a new derivation of the effective secondary emission coefficient, γ', initially proposed by Boyle and Kisliuk.[1]

II. THEORETICAL APPROACH

A. Governing equations

Under pre-breakdown conditions at moderate pressures ($p \sim 10^{-3}$-10^{2} Torr), the growth of electron current density j_e can be modeled by a first order ordinary differential equation[21]

$$\frac{dj_e}{dx} = \alpha j_e, \tag{1}$$

which is simply a steady-state, one-dimensional scalar transport equation with a source term related to Townsend's 1st ionization coefficient α. If the system is at steady state, the total current density, $j_{tot} = j_e + j_+$, is constant at any point between the cathode and anode, hence

$$\frac{dj_e}{dx} = -\frac{dj_+}{dx}, \tag{2}$$

where j_+ is the positive ion current density. Neglecting diffusion, the current density is related to the number density n and the electric field E by the drift relationship, $j = -qn\mu E$, for either species. Here, q is the unit charge and μ is the electric mobility. (The negative sign is because positive current has been defined as positive charge moving from positive x to negative x.) The electric field is described by Maxwell's equation as

$$\frac{dE}{dx} = -\frac{q}{\varepsilon_0}(n_+ - n_e), \tag{3}$$

where ε_0 is the permittivity of free space. Equation (1) is coupled to Maxwell's equation via the drift relation and through the source term αj_e because Townsend's 1st ionization coefficient, α, is a function of the electric field. Altogether, Eqs. (1)–(3) form a system of coupled, first-order ordinary differential equations that require three boundary conditions. Solving this non-linear system subject to appropriate boundary conditions, one can determine current-voltage relations, ion and electron density profiles, and electric field and potential profiles for a field emission-driven microdischarge operating in the pre-breakdown regime.

The solution domain has been defined such that the cathode is at $x = 0$ and the anode is at $x = d$. Accordingly, the total voltage drop across the gap must be

$$V_A = \int_0^d -E(x)dx = \Phi(d) - \Phi(0), \tag{4}$$

where V_A is the voltage applied across the gap and $\Phi(x)$ is the electric potential at any given point in the gap. It is also assumed that there is no net ion flux at the anode, hence the total current density at the anode is due to electrons, $j_e(d) = j_{TOT}$ or

$$j_+(d) = 0. \tag{5}$$

Classically, the total electron current density at the cathode is the sum of secondary emission where the secondary emission coefficient γ_i is assumed constant and an arbitrary background current density j_0 that is typically assumed to be photo-induced. However, at the microscale where field emission can be important, the field emission current density j_{FE} must also be included. Therefore, the cathode boundary condition is defined as

$$j_e(0) = j_{FE}(E_0) + \gamma_i j_+(0) + j_0. \tag{6}$$

The field emission current is a function of the local electric field at the cathode $E_0 = E(0)$ and here is predicted by the Fowler-Nordheim[22] equation

$$j_{FE} = C_{FN}(\beta E_0)^2 \exp\left[\frac{-D_{FN}}{\beta |E_0|}\right]. \tag{7}$$

C_{FN} and D_{FN} are constants related to the work function of the cathode material and very loosely dependant on the

electric field[23] and β is the local, geometric field-enhancement factor.[24] Up to this point, all that separates this model from a traditional Townsend dark discharge is the field emission term appearing in Eq. (6), which essentially leads to the failure of *pd* scaling, since it strongly depends on the applied electric field, V_A/d.

B. Approximate analytic solution

While the full set of coupled equations can be solved numerically, as described in the Appendix, an approximate analytical solution can provide important physical insight into the scaling that governs the discharge and how and why ion-enhanced field emission occurs. If one simply assumes the field due to space-charge is much less than the applied field, $E_{SC}(x) \ll V_A/d$ or $E(x) \approx V_A/d$, Townsend's ionization coefficient α becomes a constant and Eqs. (1)–(3) are no longer coupled. (A detailed discussion on the validity of this assumption will be presented in Sec. III) Solutions to Eqs. (1) and (2), subject to the boundary condition given by Eq. (5), are simply

$$j_e(x) = c_1 e^{\alpha x} \tag{8}$$

and

$$j_+(x) = c_1(e^{\alpha d} - e^{\alpha x}), \tag{9}$$

where c_1 is a constant of integration that is determined by applying the boundary condition at the cathode. Applying the drift relation and combining Eqs. (8) and (9) with Eq. (3), Maxwell's equation can be rewritten as

$$\frac{dE}{dx} \approx \frac{c_1}{\left(V_A/d\right)\varepsilon_0\mu_+}[e^{\alpha d} - e^{\alpha x}], \tag{10}$$

if one assumes the ion mobility is much less than the electron mobility, $\mu_+ \ll \mu_e$.[25] Integrating Eq. (10) and applying the boundary condition given by Eq. (4) yields the electric field in the domain

$$E(x) = \frac{c_1}{\left(V_A/d\right)\varepsilon_0\mu_+}\left[xe^{\alpha d} + \frac{1}{\alpha}(1 - e^{\alpha x})\right] + E_0, \tag{11}$$

where

$$|E_0| = V_A/d + \frac{c_1}{V_A\varepsilon_0\mu_+}\left[\frac{d^2}{2}e^{\alpha d} + \frac{1}{\alpha^2}(1 - e^{\alpha x}) + \frac{d}{\alpha}\right]. \tag{12}$$

For compactness, let

$$A = \frac{1}{V_A\varepsilon_0\mu_+}\left[\frac{d^2}{2}e^{\alpha d} + \frac{1}{\alpha^2}(1 - e^{\alpha x}) + \frac{d}{\alpha}\right]. \tag{13}$$

Note that the field at the cathode is the sum of the applied field and a field due to space charge, $E_{SC} = c_1 A$, where A clearly depends on the amount of ionization in the domain. At this point, the boundary condition given by Eq. (6) can be applied, yielding a transcendental equation for c_1,

$$c_1[1 - \gamma_i(e^{\alpha d} - 1)] = C_{FN}\left[\beta V_A/d + c_1 A\right]^2 \exp \times \left[\frac{-D_{FN}}{\beta V_A/d} + c_1 A\right] + j_0. \tag{14}$$

It will be shown in a later section, that a solution to this equation exists only for a certain set of parameters p, d, and V_A, and this solvability criterion can be used to determine the breakdown voltage.

Once again, utilizing the original assumption that the field due to space charge is much less than the applied field, $E_{SC} = c_1 A \ll V_A/d$, an approximate solution to Eq. (14) may be obtained. Neglecting the $c_1 A$ terms on the right hand side of Eq. (14) leads to a closed-form for c_1 and the following relations for the total current j_{TOT}, the total ion density $n_+(x)$, electron density $n_e(x)$, and the field due to ions at the cathode $E_{SC}(x = 0)$.

$$j_{TOT} = \frac{e^{\alpha d}}{1 - \gamma_i(e^{\alpha d} - 1)}\left[j_{FE}\left(\beta V_A/d\right) + j_0\right], \tag{15}$$

$$n_+(x) = \frac{(e^{\alpha d} - e^{\alpha x})}{q\mu_+\left(V_A/d\right)[1 - \gamma_i(e^{\alpha d} - 1)]}\left[j_{FE}\left(\beta V_A/d\right) + j_0\right], \tag{16}$$

$$n_e(x) = \frac{e^{\alpha x}}{q\mu_e\left(V_A/d\right)[1 - \gamma_i(e^{\alpha d} - 1)]}\left[j_{FE}\left(\beta V_A/d\right) + j_0\right], \tag{17}$$

$$E_{SC}|_{x=0} = \frac{j_{FE}\left(\beta V_A/d\right) + j_0}{1 - \gamma_i(e^{\alpha d} - 1)}A(V_A, d, p). \tag{18}$$

Note that all four of these parameters contain a factor of $[j_{FE}(\beta V_A/d) + j_0]$, and by neglecting the field emission term, j_{FE}, one obtains scaling laws for a traditional Townsend dark discharge. Also note that Eqs. (15)–(18) still contain the same singularity predicted by Paschen (i.e., $\gamma[exp(\alpha d) - 1] = 1$), and thus will lead to the traditional Paschen's curve rather than the modified Paschen's curve. This is because the field due to space charge has been neglected and the effect of ion-enhanced field emission is not captured by the approximate analytic solution. In essence, the approximate analytic solution treats field emission as a background current similar to j_0, independent of discharge properties.

In this work, the gas of interest was argon (Ar), and the ion mobility was assumed to be constant at $\mu_+ = 0.5 \times 10^{-4}$ $m^2\ V^{-1}\ s^{-1}$.[26] Important results from this model exhibit little dependence on the electron mobility as long as it is much larger than the ion mobility. (Note that Eqs. (15), (16), and (18) have no dependence on μ_e.) Hence, for the purposes of this work, it is sufficient to assume an average, constant electron mobility that is three orders of magnitude higher than the ion mobility, $\mu_e = 1000 \times \mu_+$. Townsend's first ionization coefficient is calculated using $\alpha = Cp \exp\lfloor -D\sqrt{\frac{p}{E}}\rfloor$ where $C = 2920\,\mathrm{Torr}^{-1}\ \mathrm{m}^{-1}$ and $D = 266\ \mathrm{V}^{1/2}\ \mathrm{Torr}^{-1/2}\ \mathrm{m}^{-1/2}$ for Ar.[25] The work function was assumed to be 4.65 eV and the resulting Fowler-Nordheim constants

were $C_{FN} = 3.312 \times 10^{-7}$ AV^{-2} and $D_{FN} = 6.849 \times 10^{10}$ V m^{-1}.[23] The geometric enhancement factor was set as a constant of $\beta = 55$, consistent with polished metal.[27] Studies were also conducted with nitrogen (N_2) using the appropriate gas parameters, but the results were qualitatively similar to Ar. These results are omitted here for conciseness.

III. RESULTS

A. Current-voltage relations

The total pre-breakdown current density in Ar as predicted by the analytic approximation, Eq. (15), is compared to the numeric solution to the fully-coupled system in Fig. 1. Background current j_0 has been neglected because field emission current j_{FE} quickly becomes several orders of magnitude larger as the applied potential is increased. Notably, the numerically determined current-voltage relation has an apparent singularity near 174 V, which corresponds to the breakdown voltage for that particular pressure and gap distance due to ion-enhanced field emission. Meanwhile, the approximate analytic solution given by Eq. (15) continues to increase as $\exp(\alpha d) \times j_{FE}(\beta V_A/d)$, as this equation does not capture the effect of ion-enhanced field emission on breakdown. Both results agree well up to within a few volts of breakdown for all cases tested. Importantly, these results demonstrate the validity of the approximate solution for applied potentials *below* the breakdown threshold. That is to say, one can treat the discharge as a normal Townsend dark discharge where primary cathode electrons—or background current—are provided by field emission. In a traditional Townsend dark discharge, secondary emission and electron impact ionization multiply background current from the cathode by a factor

$$M = \frac{e^{\alpha d}}{1 - \gamma_i(e^{\alpha d} - 1)}. \tag{19}$$

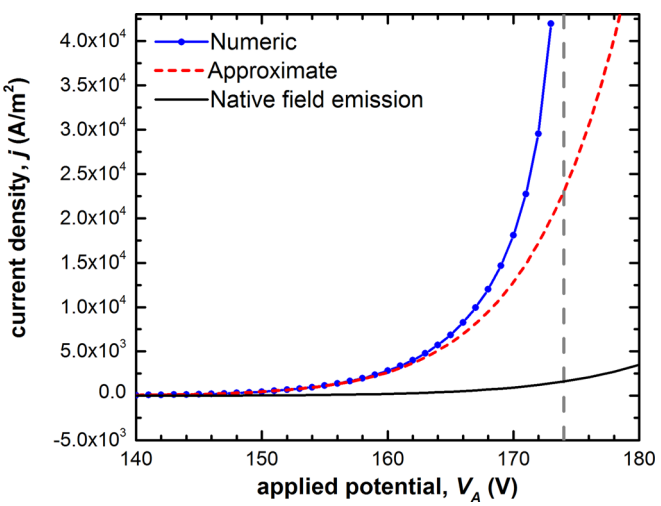

FIG. 1. Current density j as a function of applied potential V_A in argon for $p = 760$ Torr and $d = 3$. Three cases are shown: native field emission using the Fowler-Nordheim equation (Eq. (8)) and only the applied electric field, the current density as predicted by the approximate analytic solution (Eq. (15)), and the numeric solution for the current density. The vertical dash line represents the numerically calculated breakdown voltage, $V_b = 174$ V.

In Fig. 2, dividing the numeric solution by native field emission, $j_{FE}(\beta V/d)$, and comparing it to Eq. (19), one can see how field emission current is simply multiplied by traditional electron avalanche processes until the buildup of positive space increases the electric field at the cathode by an appreciable amount. Because field emission responds to the summation of the applied field *and* the space charge field, the field emission current is enhanced due to the build up of positive space charge, which increases the field at the cathode. The approximate model neglects the field due to space charge and therefore does not capture this effect.

B. Space charge and the electric field

It has been suggested that breakdown in microscale gaps is similar to vacuum breakdown because the mean free path between ionizing collisions is on the order of the gap size.[4] Hence, one can assume there are few ionizing collisions in the gap. This would be true for a *macroscale* gap with very small, constant background current density, $j_0 \sim 10^{-10}$ A m^{-2}, where pre-breakdown parameters scale as $j_0 \times \exp(\alpha d)$. However, due to the presence of field emission in a *microscale* gap, the "background" current density is effectively the native field emission, $j_{FE}(\beta V_A/d)$, which grows exponentially with applied potential to values on the order of 10^3 A m^{-2} or higher.[28] When field emission becomes strong, there is a great abundance of seed electrons from the cathode to produce ions in the gap. Hence, though electron multiplication is modest ($\exp(\alpha d) \sim$ 1-10), large ion ($\sim 10^{13}$ cm^{-3}) and electron ($\sim 10^{10}$ cm^{-3}) densities are produced in this field emission-driven, Townsend dark discharge. This effect has been experimentally observed in the design of ionizing devices for mass spectrometry and gas sensing, but never fully explained.[17–20] In Fig. 3, the approximate analytic solution for the ion density near the cathode, $n_{+,0} = n_+(0)$, using Eq. (16), is plotted as a function of applied voltage for various gap sizes. One can see that relatively high cathode ion densities ($\sim 10^{12}$-10^{14} cm^{-3}) are attainable at fairly low voltages.

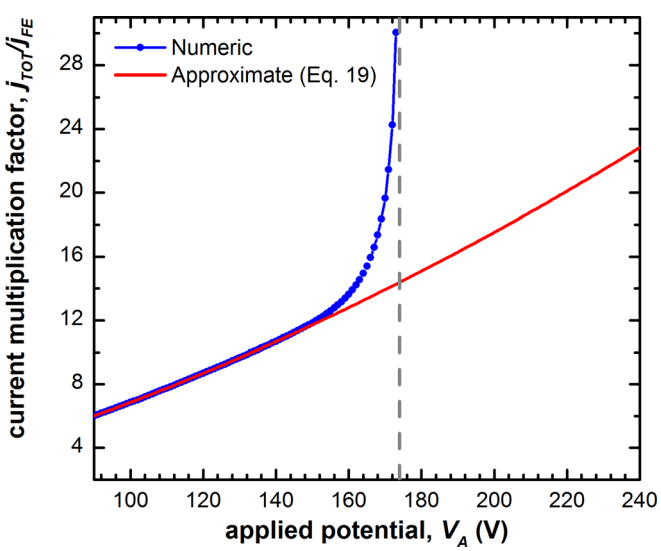

FIG. 2. Total current density divided by native field emission j_{TOT}/j_{FE} as a function of the applied potential V_A in argon for $p = 760$ Torr and $d = 3$ μm. The vertical dash line represents the numerically calculated breakdown voltage, $V_b = 174$ V.

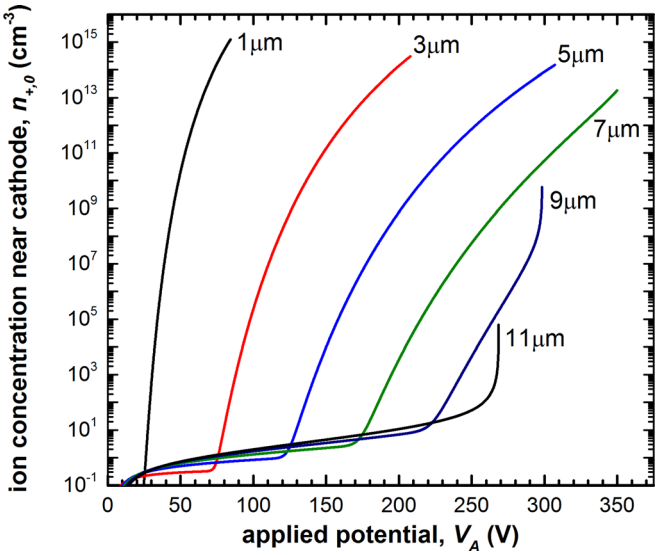

FIG. 3. Approximate ion concentration at the cathode $n_{+,0}$ using Eq. (16) for gap sizes from $d = 1$–11 μm in argon at $p = 760$ Torr with background current $j_0 = 10^{-10}$ A m^{-2}. Curves have been truncated when $E_{SC} \geq 0.1 V_A/d$.

The abrupt singularities for the larger gaps on the right correspond to traditional Paschen breakdown as discussed previously.

In Fig. 4, the approximate analytic solution given by Eq. (16) for $n_{+,0}$ is compared to the numerically computed ion concentration near the cathode as a function of V_A. Similar to the total current, both agree well up to within a few volts of breakdown at which the numeric result diverges to infinity at the field emission-induced breakdown voltage, while the approximate solution continues to increase as $\exp(\alpha d) \times j_{FE}(\beta V/d)$. However, because the two solutions agree well for ion densities as high as 1×10^{13} cm^{-3}, one must conclude that ion densities below this magnitude do not significantly alter the applied field and the validity of the assumption made when deriving the analytic solution $E_{SC} \ll V_A/d$ is maintained. With simple scaling analysis of the one-dimensional Poisson equation, one can easily see how this is the case.

Consider the non-dimensional variables $\varphi = \Phi/V_A$ and $X = x/d$, which essentially normalize the boundary conditions to unity. The one-dimensional Poisson's equation then becomes

$$\frac{\partial^2 \phi}{\partial X^2} - \frac{qd^2}{V_A \varepsilon_0}(n_e - n_+). \tag{20}$$

The electron density can be neglected because of the high electron mobility. Accordingly, solutions to Eq. (20) will be approximately harmonic (in this case linear) if the non-dimensional parameter, $qd^2 n_+/V_{AP}\varepsilon_0$, is much less than one,

$$\frac{qd^2 n_+}{V_A \varepsilon_0} \ll 1 \rightarrow \frac{qd^2 n_+}{V_A \varepsilon_0} \leq 0.1. \tag{21}$$

Considering the upper limit of this strong inequality, one finds the critical ion density necessary to significantly distort the electric field to be $n_+ \approx 0.1 V_A \varepsilon_0/qd^2$. Plugging in values of $d = 3\,\mu$m and $V_A = 150$ V indicates that ion densities must be on the order of 10^{13} cm^{-3} or higher to yield any appreciable distortion of the applied electric field. This agrees well with the divergence of the numeric solution from the approximate analytic solution seen in Fig. 4.

Shown in Fig. 5, the field due to space charge E_{SC} at the cathode as a function of applied potential was calculated numerically for a 3 μm gap and compared to the approximate analytic solution given by Eq. (18). Similar to total current, the numeric solution for the electric field at the cathode has an apparent singularity at the breakdown voltage, while the approximate solution continues to increase proportional to $V_A^{-1} \times j_{FE}(\beta V_A/d)$. Both agree fairly well for applied potentials up to within a few volts of breakdown. Once again, note that the divergence of the numeric solution from the approximate solution near $V_A = 168$ V corresponds to an ion density in Fig. 4 on the order of 10^{13} cm^{-3} as predicted by the

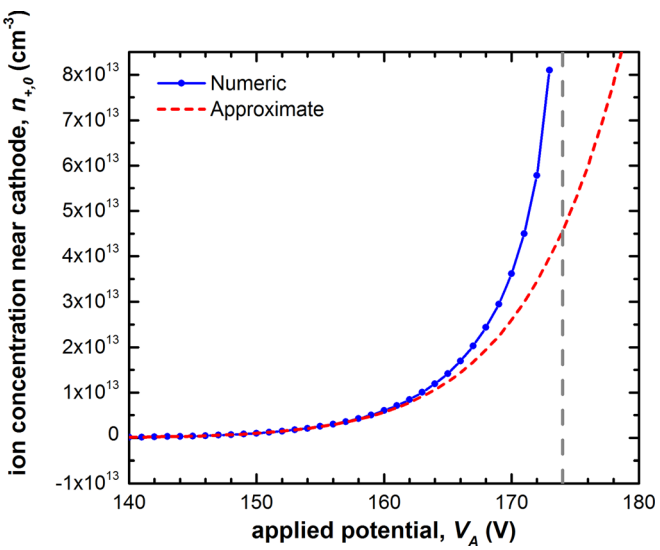

FIG. 4. Ion concentration at the cathode $n_{+,0}$ in Ar for $p = 760$ Torr and $d = 3\,\mu$m. The vertical dash line represents the numerically calculated breakdown voltage, $V_b = 174$ V.

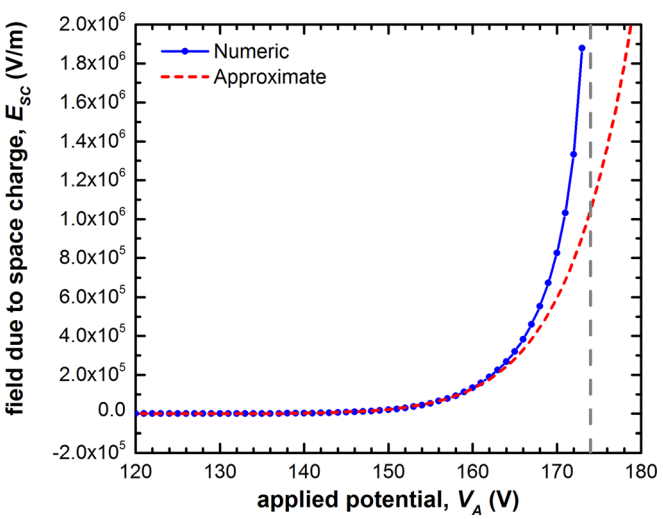

FIG. 5. Electric field due to space charge at the cathode $E_{SC}(x = 0)$ in Ar for $p = 760$ Torr and $d = 3\,\mu$m. The vertical dash line represents the numerically calculated breakdown voltage, $V_b = 174$ V.

scaling analysis in Sec. III B. Interestingly enough, the two solutions quickly begin to diverge when the field due to space charge grows to within 1% of the applied field. The rapid divergence to infinity for all parameters when the field due to space charge reaches 1% of the applied field is due to the exponential scaling of the $j_{FE}(E_0)$ term that couples all of these parameters via the boundary condition at the cathode.

C. Breakdown voltages

Paschen's original criterion for breakdown is given by the well-known relation

$$\lambda(e^{\alpha d} - 1) = 1. \tag{22}$$

This equation has both a physical and mathematical interpretation. From a strictly mathematical perspective, this is simply a singularity in the avalanche multiplication factor given by Eq. (19). It can also be viewed as a *solvability* condition on the boundary condition at the cathode. Neglecting the field emission term on the right-hand side of Eq. (14), one can see that a physical solution for c_1 does not exist if $\gamma[\exp(\alpha d) - 1] \geq 1$. From a *physical* perspective, Eq. (22) represents a *self-sustained* condition. That is, the number ions required to emit a secondary electron from the cathode, $1/\gamma$, is equal to the number of ions produced by an emitted electron via an avalanche $[\exp(\alpha d) - 1]$.

From a purely mathematical perspective, the criterion for *microscale* breakdown where *field emission is active* also manifests itself as a solvability condition on the boundary condition at the cathode given by Eq. (14) for the constant of integration c_1. In Figure 6, the left and right hand side of Eq. (14) are plotted as function of c_1, one can see that for certain values of V_A, d, and p, solutions do not exist. For a given pressure p and gap distance d the breakdown voltage V_B can be determined as the largest applied voltage for which a solution to Eq. (14) still exists. For large gap distances ($d > 10\,\mu$m), the field emission term becomes negligible and one recovers Paschen's law.

From a physical perspective, *microscale* breakdown can be defined in terms of the critical ion density necessary to significantly distort the electric field and enhance field emission—that is, the point where the feedback mechanism between ionization and field emission becomes significant. As shown in Secs. III A and III B, the numerical results begin to rapidly diverge to infinity when a critical ion density, $n_+ \approx 0.1 V_A \varepsilon_0 / q d^2$, is reached. Setting the ion density given by Eq. (16) equal to this critical ion density yields the following criterion for breakdown

$$1 = \left[\gamma_i + \frac{10 C_{FN} \beta^2 d}{\varepsilon_0 \mu_+} \exp\left(\frac{-D_{FN} d}{\beta V_A}\right)\right](e^{\alpha d} - 1). \tag{23}$$

This equation is equivalent to the pseudo-analytic form presented by Go and Pohlman[29] containing the effective secondary emission coefficient, $\gamma' = K\exp(-B/E_A)$, that was originally suggested by Boyle and Kisliuk[1] and implemented by Radmilović and Radjenović,[30] where the non-physical fitting parameter K has now been analytically determined to be

$$K = \frac{10 C_{FN} \beta^2 d}{\varepsilon_0 \mu_+}. \tag{24}$$

As noted in prior work by Go and Pohlman,[29] the factor K has previously never been *explicitly* related to any physical parameters and in many ways has been used as an ill-defined fitting parameter. When extracted from other models, the value typically takes a magnitude of $K \sim 10^7$, but the physical plausibility of this value has remained elusive. However, using Eq. (24), it can be calculated as $K = 6.79 \times 10^7$ for a $3\,\mu$m gap, which is directly inline with previous approximations.

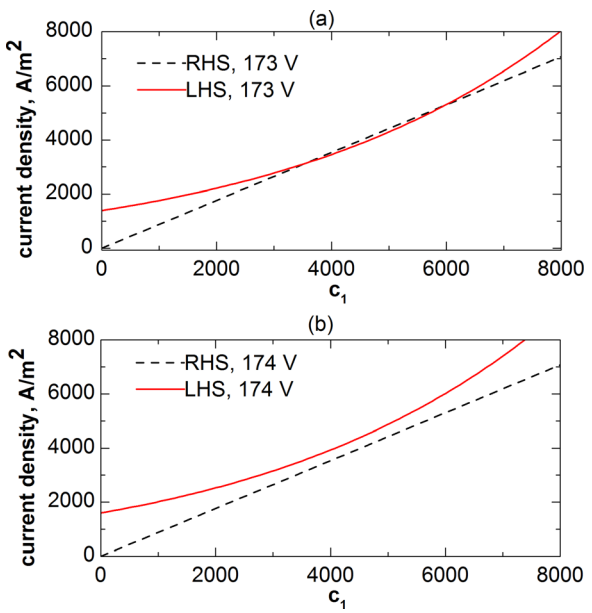

FIG. 6. Plots of the left (LHS) and right hand side (RHS) of Eq. (14) for Ar at $p = 760$ Torr and $d = 3\,\mu$m. (a) A solution clearly exists for an applied potential of 173 V where the two curves intersect. (b) A solution does not exist for applied potentials of 174 V and higher, as the two curves diverge.

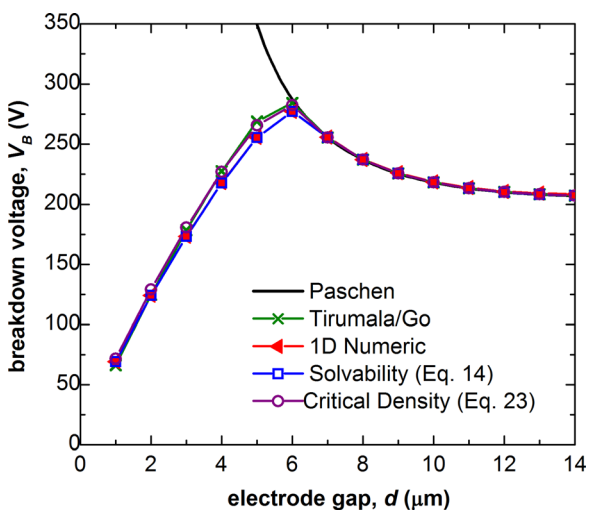

FIG. 7. Computed breakdown voltages in Ar at $p = 760$ Torr, $\phi = 4.65$ eV, and $\beta = 55$. The traditional Paschen's curve is compared to the theory of Tiumala and Go,[6] numerical solutions to Eqs. (1)–(3), the solvability condition on Eq. (14), and the form due to the critical density given by Eq. (23).

Figure 7 shows breakdown voltages determined from the approximate analytical solution, numeric solution, and the condition defined in Eq. (23) as well as those using the analytical model of Tirumala and Go.[6] All the schemes agree extremely well with one another, showing that there are multiple theoretical approaches to field emission-induced breakdown phenomena, each revealing their own insights. Further, for large gap distances ($d > 10\,\mu m$), the field emission term becomes negligible, and all four models converge to Paschen's curve.

IV. CONCLUSIONS

Basic scaling laws have been derived analytically using a one-dimensional fluid model for field emission-driven Townsend microdischarges. These scaling laws are equivalent to a classic Townsend dark discharge where field emission behaves as a background current that provides seed electrons to initiate an avalanche. This approximate analytic model is valid for applied potentials up to within a few volts of breakdown, at which point ion-enhanced field emission begins to play a significant role. Unlike macroscale gaps, the presence of field emission in a microdischarge provides a large source of cathode electrons that create an abundance of ions in the gap through ionizing collisions. When positive space charge densities in the gap become sufficiently large, the electric field at the cathode is increased and field emission current increases. Simple scaling analysis shows that the critical ion concentration necessary to significantly enhance the electric field at the cathode is approximately $n_+ \approx 0.1 V_A \varepsilon_0 / q d^2$. Setting the approximate analytic relation for the ion concentration at the cathode equal to this critical density yields the effective secondary emission coefficient, γ', originally suggested by Boyle and Kisliuk.

It should be noted that there are challenges/limitations to be considered when applying this model to any experiment using conventional metallic electrodes. Several publications have shown experimentally that a thin oxide layer can significantly inhibit field emission and a sudden breakdown or removal of this oxide layer—often referred to as activation of the surface—can lead to a sudden jump in field emission current, which could easily be interpreted as gaseous breakdown.[31] Further, considering the large ion concentrations predicted by this model, one would expect cathode erosion to play a significant role, leading to instabilities in the field emission parameter β as well as the active emission area.[32] The model can potentially account for these material effects with the proper selection of ϕ and β. Additionally, long path effects[7] must also be mitigated during experiments, including careful control of the electrode shape and vessel, in order to properly observe field emission that corresponds to this 1D model, rather than other anomalous phenomena. Although this work only considers the particular case of metallic electrodes with a $3\,\mu m$ gap, the model could also be applied to a larger scale discharge ($\sim 50\,\mu m$) utilizing an unconventional cathode material with a much larger β (~ 1000) such as carbon nanotubes. In particular, it could potentially explain the low sustaining voltages and the pressure scaling of the current-voltage curves reported in Refs. 11 and 17. To that end, the next step in continuing the study of field emission-driven Townsend discharges must be carefully structured and controlled experiments.

ACKNOWLEDGMENTS

This material is based upon work supported by the Air Force Office of Scientific Research under AFOSR Award No. FA9550-11-1-0020.

APPENDIX: NUMERICAL SCHEME

The full, non-linear system of coupled equations has also been solved numerically using an iterative, second-order finite difference scheme on a uniform grid. Initially, a linear potential and constant electric field are assumed ($E(x) = V_A/d$). Heun's method is used to solve Eq. (1) for the electron current at each discretized node i

$$j_{e,i+1} = j_{e,i+1} + \frac{\Delta x}{2}\left[\alpha_i j_{e,i} + \alpha_{i+1}\left(j_{e,i} + \Delta x \alpha_i j_{e,i}\right)\right] \tag{A1}$$

and the ion current at each point is calculated as the total current less the electron current

$$j_{+,i} = j_{tot} - j_{e,i} = j_{e,N} - j_{e,i}. \tag{A2}$$

The number density n and subsequent charge density, $\rho = qn$, at each point are then determined from current density using the drift relation $j = -qn\mu E$. The electric potential Φ and electric field E are re-computed using the charge density via a second-order finite difference scheme

$$\Phi_i = \frac{1}{2}\left[\frac{\rho i (\Delta x)^2}{\varepsilon_0} + \Phi_{i-1} + \Phi_{i+1}\right], \tag{A3}$$

$$E_i = \frac{\Phi_{i-1} - \Phi_{i+1}}{2\Delta x}, \tag{A4}$$

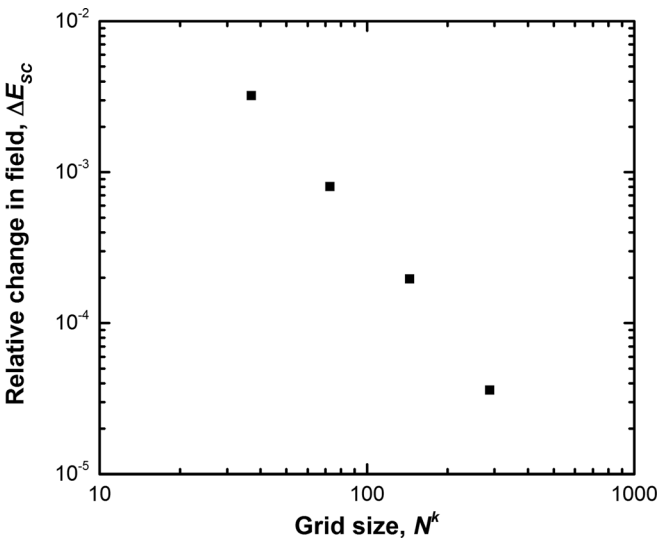

FIG. 8. Grid convergence test for argon at $p = 760$ Torr, $d = 3\,\mu m$, and $V_A = 102$ V. When the grid size is increased from 145 to 289 grid points, the converged field due to space charge at the cathode changes by less than 0.005%.

where Δx is the distance between adjacent grid points. Second order forward and backward derivatives are used to calculate the electric field at the cathode and anode, respectively. The newly calculated field and potential are then used to re-solve Eq. (1) and the entire process is repeated until the total current changes by less than 0.1% and the field due to space charge at the cathode changes by less than 0.1% between consecutive iterations.

A grid convergence test was performed to insure grid-independence of numeric solutions. In this test, the number of grid points N^k was iteratively doubled, and the relative change in the space charge field at the cathode, $E_{SC} = E_0 - E_A$, was taken between successive grids according to the formula

$$\Delta E_{SC} = \left| \frac{E_0^{K+1} - E_0^K}{E_0^k - E_{AP}} \right|, \tag{A5}$$

where k is the index of the grid size. Approximately doubling the number of grid points with each iteration such that $N^{k+1} = 2N^k - 1$ allowed for direct comparison of corresponding grid points without interpolation. The results of this test are shown below in Fig. 8. When the grid size is increased from 145 to 289 grid points, the converged field due to space charge at the cathode changes by less than 0.005%.

[1]W. S. Boyle and P. Kisliuk, Phys. Rev. **97**, 255 (1955).
[2]K. H. Becker, K. H. Schoenbach, and J. G. Eden, J. Phys. D: Appl. Phys. **39**, R55 (2006).
[3]D. Mariotti and R. M. Sankaran, J. Phys. D: Appl. Phys **43**, 323001 (2010).
[4]P. G. Slade and E. D. Taylor, IEEE Trans. Compon. Packag. Technol. **25**, 390 (2002).
[5]M. Radmilović-Radjenović and B. Radjenović, IEEE Trans. Plasma Sci. **35**, 1223 (2007).
[6]R. Tirumala and D. B. Go, Appl. Phys. Lett. **97**, 151502 (2010).
[7]D. Marić, N. Škoro, P. D. Maguire, C. M. O. Mahoney, G. Malović, and Z. L. Perović, Plasma Sources Sci. Technol. **21**, 1 (2012).
[8]G. J. Kim, F. Iza, and J. K. Lee, Phys. Plasma **16**, 013502 (2009).
[9]C. J. Wagner, P. A. Tchertchian, and J. G. Eden, Appl. Phys. Lett. **97**, 134102 (2010).
[10]P. A. Tchertchian, C. J. Wagner, T. J. Houlahan, B. Li, D. J. Sievers, and J. G. Eden, Contrib. Plasma Phys. **51**, 889 (2011).
[11]S. J. Park and J. G. Eden, Appl. Phys. Lett. **84**, 4481 (2004).
[12]A. Allen, A. Cannon, L. Jengchul, W. P. King, and S. Graham, J. Micromech. Microeng. **16**, 2722–2729 (2006).
[13]M. S. Peterson, W. Zhang, T. S. Fisher, and S. V. Garimella, Plasma Sources Sci. Technol. **14**, 654 (2005)
[14]D. B. Go, T. S. Fisher, S. V. Garimella, and V. Bahadur, Plasma Sources Sci. Technol. **18**, 035004 (2009).
[15]A. Venkattraman, A. Garg, D. Peroulis, and A.A. Alexeenko, Appl. Phys. Lett. **100**, 083503 (2012).
[16]E. Hourdakis, B. J. Simonds, and N. M. Zimmerman, Rev. Sci. Instrum. **77**, 034702 (2006).
[17]R. B. Sadeghian and M. Kahrizi, in IEEE Sensors 2007 Conference (IEEE, 2007), p. 648.
[18]Z. Hou, H. Liu, X. Wei, J. Wu, W. Zhou, Y. Zhang, X. Dong, and B. Cai, Sens. Actuators, B **127**, 637–648 (2007).
[19]J. Kim, Phys. D: Appl. Phys. **39**, 3026–3029 (2006).
[20]O. Kornienko, P. T. Reilly, W. B. Whitten, and J. M. Ramsey, Anal. Chem. **72**, 559 (2000).
[21]J. S. Townsend, Nature **62**, 340 (1900).
[22]R. H. Fowler and L. Nordheim, Proc. Roy. Soc. London **119**, 173 (1928).
[23]W. W. Dolan, Phys. Rev. **91**, 510 (1953).
[24]T. J. Lewis, J. Appl. Phys. **26**, 1405 (1955).
[25]Y. P. Raizer, *Gas Discharge Physics* (Springer-Verlag, Berlin, 1987).
[26]H. W. Ellis, R. Y. Pai, and E. W. McDaniel, At. Data Nucl. Data Tables **17**, 177–210 (1976).
[27]P. A. Chatterton, Proc. Phys. Soc. **88**, 231 (1966).
[28]W. A. de Heer, A. Châtelain, and D. Ugarte, Science **270**, 1179 (1995).
[29]D. B. Go and D. A. Pohlman, J. Appl. Phys. **107**, 103303 (2010).
[30]M. Radmilović-Radjenović and B. Radjenović, Plasma Sources Sci. Technol. **17**, 024005 (2008).
[31]S. Xavier, S. Mátéfi-Tempfli, E. Ferain, S. Purcell, S. Enouz-Védrenne, L. Gangloff, E. Minoux, L. Hudanski, P. Vincent, J. P. Schnell, D. Pribat, L. Piraux, and P. Legagneux, Nanotechnology **19**, 1–7 (2008).
[32]A. P. Janssen and J. P. Jones, J. Phys. D: Appl. Phys. **4**, 118 (1971).